RSC Advances

PAPER

View Article Online
View Journal | View Issue

Cite this: *RSC Adv.*, 2015, **5**, 13985

Silica aerogel-supported cobalt nanocomposites as efficient catalysts toward hydrogen generation from aqueous ammonia borane†

Pin-Ju Yu,[a] Mu-Hsin Lee,[a] Hung-Ming Hsu,[a] Huei-Mei Tsai[b] and Yui Whei Chen-Yang*[a]

Received 6th November 2014
Accepted 21st January 2015

DOI: 10.1039/c4ra14002h

www.rsc.org/advances

In this study, a mesoporous silica aerogel-supported cobalt (Co/SAG) nanocomposite synthesized by a facile chemical reduction was used as an alternative catalyst for hydrogen generation from aqueous NH_3BH_3. The result showed that Co/SAG exhibited 41% higher hydrogen generation rate for the NH_3BH_3 hydrolysis than the ordered mesoporous silica (MCM-41)-supported Co catalysts (Co/MCM-41) prepared by the same reduction method. This is attributed to the fact that the Co nanoparticles were smaller (less than 5 nm in diameter) and better-deposited in SAG than MCM-41 as observed in the TEM micrographs. It is also found that the Co/SAG catalyst delivered superior turnover frequency (3013 ml H_2 min^{-1} g_{metal}^{-1}) and activation energy (46.4 kJ mol^{-1}) than most of the Co-based catalysts reported. This study showed that the Co/SAG prepared is a potential non-precious catalyst for hydrogen generation from aqueous NH_3BH_3.

1. Introduction

With the increasing demand for a sustainable and clean energy supply, hydrogen is considered to be one of the alternative energy sources as compared to fossil fuels.[1] Over the past decades, hydrogen has been commonly stored in tanks as compressed or liquefied form,[2] on carbon materials,[3–5] hydrogen-absorbing alloys,[6,7] and metal–organic frameworks,[8] but their volumetric and gravimetric efficiencies are still too low to make them practically feasible. Therefore, searching for reliable and efficient methods for hydrogen storage is essential for the future hydrogen economy. Recently, ammonia borane (NH_3BH_3) with nontoxic, stable and eco-friendly features has been recognized as an attractive candidate for hydrogen storage applications because of its gravimetric hydrogen capacity (19.6 wt%), high solubility and demonstrated stability in neutral aqueous solutions.[9] To generate hydrogen from ammonia borane, several approaches, including solid-phase thermolysis,[10] catalytic dehydrogenation in non-aqueous solvents,[11] and hydrolysis,[12] have been reported. Among them, the hydrolysis appeared to be one of the best ways because with appropriate catalysts it can deliver 3 mol H_2 per mol of NH_3BH_3 at room temperature.[13] The hydrolysis of ammonia borane can be expressed in equation:

$$NH_3BH_{3(s)} + 2H_2O_{(l)} \rightarrow NH_4^+{}_{(aq)} + BO_2^-{}_{(aq)} + 3H_{2(g)}$$

The precious metal-based catalysts such as Pt, Pd, Ru, and Rh have been found to be effective for accelerating the hydrolysis of ammonia borane, but they are not suitable for practical applications due to their limited resources and high cost.[14–17] Therefore, numerous efforts have been made to develop the efficient and economical non-noble metal-based catalysts[18–25] in element forms *e.g.* Fe, Co, Ni, Cu or supported forms on γ-Al_2O_3, SiO_2, carbon, *etc.* supports. Silica aerogels are materials that can comprise as high as 96% porosity, while the remaining 4% is a network structure of silicon dioxide. Due to their unique characteristics, such as high porosity, large surface area, low density and low thermal conductivity, silica aerogels have been used as advance materials in the applications of thermal insulation, electrical batteries, nuclear waste storage, catalysis, acoustic insulation, adsorbents, *etc.*[26]

In this study, mesoporous silica aerogel-supported Co nanocomposite (Co/SAG) was synthesized by the facile chemical reduction method for use as an alternative catalyst for hydrolysis of ammonia borane. For comparison, the ordered mesoporous silica (MCM-41)-supported Co nanocomposite (Co/MCM-41) was prepared by the same reduction method. The crystalline structure, morphology, chemical composition and porous characteristic of the catalysts prepared were

[a]*Department of Chemistry, Center for Nanotechnology and Center for Biomedical Technology, Chung Yuan Christian University, Chung-Li 32023, Taiwan, Republic of China. E-mail: yuiwhei@cycu.edu.tw; Tel: +886-3-2653317*

[b]*Materials and Electro-Optics Research Division, Electric Energy Section, Chung Shan Institute of Science and Technology, Lung-Tan 32544, Taiwan, Republic of China*

† Electronic supplementary information (ESI) available: EDX of (a) Co/SAG and (b) Co/MCM-41. The plot of hydrogen generation rate *versus* the concentration of AB. See DOI: 10.1039/c4ra14002h

characterized by X-ray diffraction (XRD), transmission electron microscopy (TEM), inductively coupled plasma-atomic emission spectrometer (ICP-AES) and nitrogen adsorption–desorption analyzer. The rates and activation energies for hydrolysis of ammonia borane catalyzed by the as-prepared Co/SAG catalyst at various temperatures and ammonia borane concentrations were evaluated and compared with that by the Co/MCM-41 catalyst. To the best of our knowledge, it is the first study to employ mesoporous silica aerogels as supporting material to synthesize Co-based catalysts and explore the influence of morphology on Co-based catalysts towards hydrolysis of ammonia borane.

2. Experimental

2.1 Chemicals

All chemicals, including cetrimonium bromide (CTAB, 99%, Acros Organics), tetraethoxysilane (TEOS, 98%, Acros Organics), ammonium hydroxide (NH_4OH, 99.8%, Pharmco), cobalt(II) nitrate hexahydrate ($Co(NO_3)_2 \cdot 6H_2O$, 98%, Alfa Aesar), sodium borohydride ($NaBH_4$, 99%, Aldrich), ammonia borane (NH_3BH_3, 97%, Aldrich) were used as received.

2.2 Preparation of mesoporous silica aerogel (SAG)

The SAG was prepared by the sol–gel process from the silicon precursor, TEOS, using 1-butyl-3-methylimidazolium tetrafluoroborate (BMIBF) as the template and solvent (methanol) as reported.[27] The processes are described as follows: BMIBF (3.0 g), methanol (1.9 g) and deionized water (3.4 g) were mixed in a bottle then the designated stoichiometric ratio amount of TEOS (5.8 g) was added. A homogeneous gel was formed by gelation at room temperature within 1 h after mixing and aged at ambient temperature for 2 days in the open air. Then the entrapped ionic liquid was Soxhlet-extracted with ethanol for 2 days. The SAG was finally obtained by freeze-drying under 15 Pa at 223 K for 12 h with the freeze-dryer (Eyela FDU-1200, Tokyo Rikakikai, Japan).

2.3 Preparation of ordered mesoporous silica (MCM-41)

The MCM-41 powder was synthesized according to the published method from an alkaline solution containing CTAB, TEOS, NH_4OH as catalyst and deionized water.[28] For a typical procedure, CTAB was well dissolved into NH_4OH aqueous solution and then TEOS was successively added to the above mixture. The precursor solution was continuously stirred at 363 K for 24 h, where the molar ratio of CTAB : TEOS : NH_4OH : H_2O was kept at 1.0 : 4.5 : 54 : 620. The resulting suspension was filtered and washed with deionized water at least three times. To ensure the CTAB was completely removed, the dried powders were finally calcined in an air atmosphere at 823 K for 6 hours, yielding the ordered MCM-41.

2.4 Synthesis of Co-based catalysts, Co/SAG and Co/MCM-41

To synthesize the Co-based catalysts, a facile chemical reduction using $NaBH_4$ as reducing agent was utilized as illustrated in Scheme 1.[29] A desired amount of SAG or MCM-41 was homogeneously dispersed in the Co precursor solution by an ultrasonic processor (Sonicator S-4000, Misonix, USA) under the amplitude of 20% for 30 minutes (Step I). Afterward, 15 wt% of the freshly prepared $NaBH_4$ aqueous solution was slowly added dropwise to reduce the Co^{2+} (Step II). The Co-based catalysts separated from the black suspension by centrifuge (CN-830, Hsiang-Tai Machinery Industry Co., Ltd., Taiwan) under 3000 rpm were finally freeze-dried under 15 Pa at 223 K for 1 day (Step III). The amounts of Co deposited on Co/SAG and Co/MCM-41 were 24 wt% and 23 wt%, respectively, as determined by an inductively coupled plasma-atomic emission spectrometer (ICP-AES, ICAP 9000, Jarrell-A).

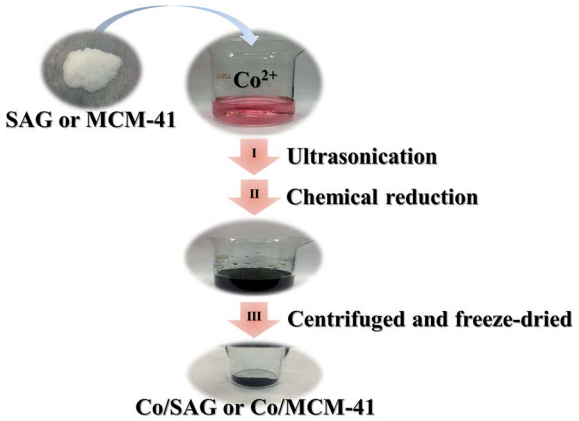

Scheme 1 Illustration of Co-based catalysts synthesis by a facile chemical reduction using $NaBH_4$ as reducing agent.

2.5 Characterizations

To identify the crystalline structure of the Co-based catalysts, a powder X-ray diffractometer (PXRD, Bruker D2 PHASER) with a Cu target ($\lambda = 1.541$ Å) excited at 30 kV and 10 mA was conducted to record their corresponding PXRD patterns of Co/SAG and Co/MCM-41 from 10° to 60°. The microstructure of the Co/SAG and Co/MCM-41 were examined by the transmission electron microscopy (TEM, JEOL Ltd., TEM-2010) at 200 kV. The pore volume, pore size distribution, and Brunauer–Emmett–Teller (BET) surface area of the SAG, MCM-41, Co/SAG and Co/MCM-41 powders were determined by a nitrogen adsorption–desorption analyzer (Tristar 3000, Micromeritics) at 77 K.

2.6 Hydrogen generation experiment

The hydrogen generation experiments were performed by using the water displacement method.[30] A weighed catalyst with metal/NH_3BH_3 molar ratio = 0.05–0.2 was first placed in a twin-necked round-bottom flask (25 ml) and the flask was then sealed with an outlet tube for collecting the generated hydrogen. An aqueous NH_3BH_3 solution (5 ml) with the designated concentration (0.33–5 wt%) was loaded into a flask, which was immersed into a water bath to maintain the constant temperature. The outlet tube exhaust was placed under an inverted, water-filled gas burette that was situated in a water-

filled vessel to monitor the volume of the displaced water, which corresponded to the volume of released hydrogen. For recycling test, the used catalysts were collected and the hydrogen generation was repeated with the same procedures as described above.

3. Results and discussion

3.1 Characterization of Co/SAG and Co/MCM-41

After the reduction process, both SAG and MCM-41 were changed from white to black as shown in Scheme 1, implying that the Co nanoparticles were successfully deposited on the SiO_2 supports *via* the chemical reduction. The loading amount of Co on Co/SAG (24 wt%) determined by the ICP-AES measurement was slightly higher than that on Co/MCM-41 (23 wt%), but both were quite close to the theoretical value (25 wt%), revealing that the method used is an efficient reduction for preparation of the Co nanoparticles on the silica-supports.

The powder X-ray diffraction patterns of the mesoporous silicas, SAG and MCM-41, were measured and shown in Fig. 1(a). No peak was found for SAG at small angle range, indicating that SAG was an amorphous material. However, the pattern in the mall angle range of MCM-41 showed three well-resolved peaks, indexed as (100), (110), and (200) diffractions, confirming the hexagonal structure as reported.[28] The Co-based catalysts were also analyzed by the powder X-ray diffraction measurements and the corresponding patterns are depicted in Fig. 1(b). Similar to that for SAG and MCM-41, the broad peaks at the Bragg angles (2θ) of $\sim$23.5° for both Co/SAG and Co/MCM-41 are assigned to the SiO_2 supports.[27] Because the (1 1 1) plane of the pure cubic phase of Co assigned by JCPDS 15-0806 is at $2\theta = \sim$21.8°, it is reasonable to believe that the Co (1 1 1) peak was overlapped with that of the SiO_2, but is difficult to determine the Co phase.[29]

The transmission electron microscopy (TEM) micrographs of Co/SAG and Co/MCM-41 were measured for the microstructural investigation and are displayed in Fig. 2. The dark spots on the silica supports are recognized as the reduced Co particles deposited. It shows that the Co nanoparticles were quite homogenously deposited among the mesopores of Co/SAG with particle sizes less than 5 nm (Fig. 2(a)). On the contrary, larger Co nanoparticles (red circled) with particle sizes of 13–20 nm are observed on the surface of Co/MCM-41 in Fig. 2(b). The formation of the smaller Co nanoparticles in Co/SAG is attributed to the network structure of SAG,

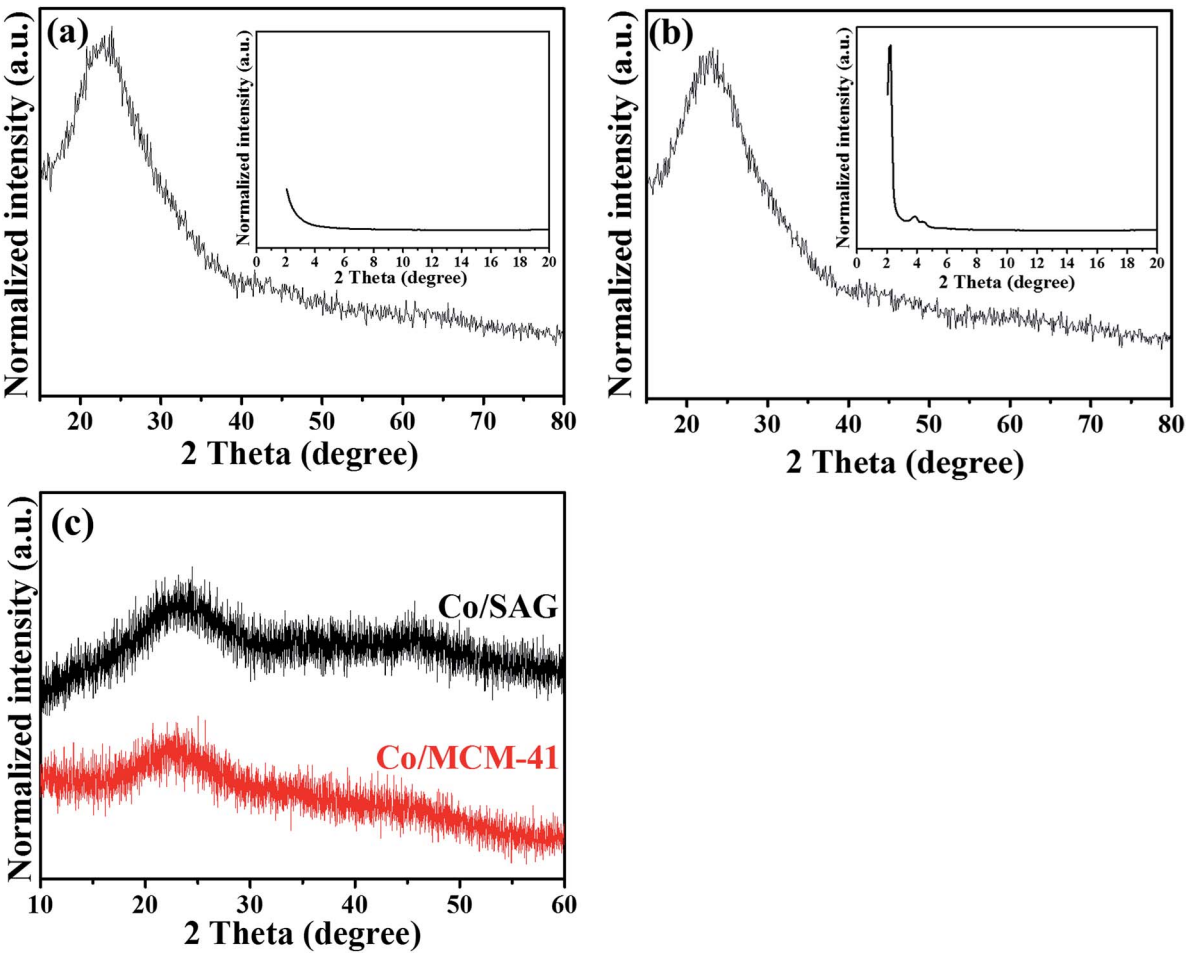

Fig. 1 PXRD patterns of (a) SAG, (b) MCM-41 and (c) Co/SAG and Co/MCM-41.

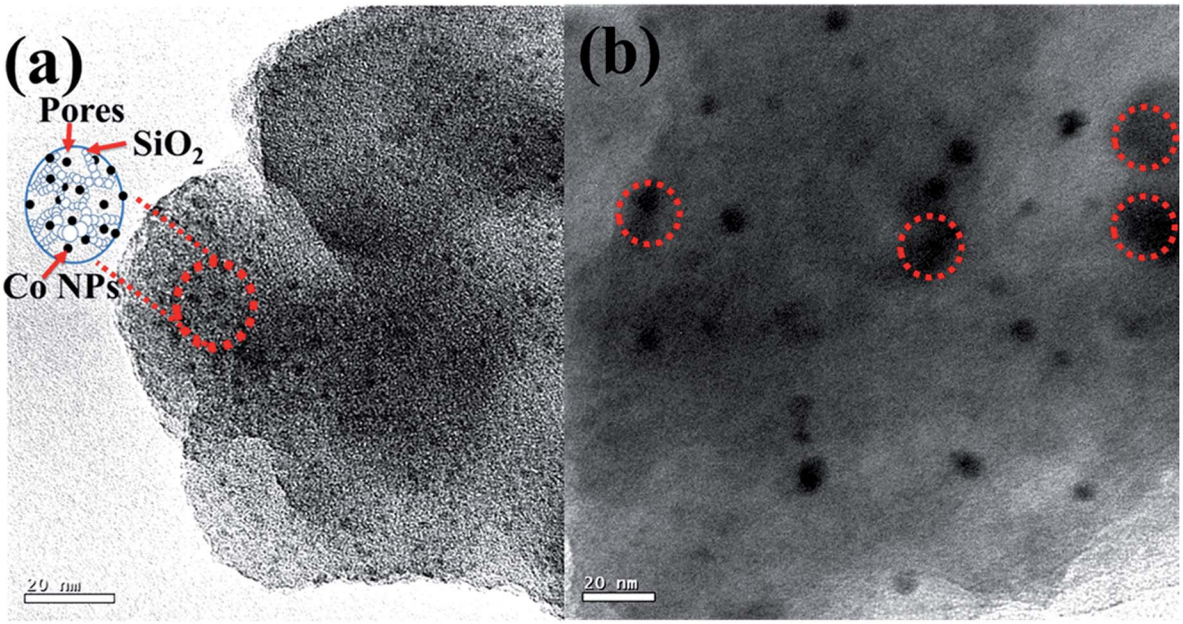

Fig. 2 TEM micrographs of (a) Co/SAG and (b) Co/MCM-41, scale bar: 20 nm.

providing more sites for deposition of the reduced Co-nanoparticles and the interconnected mesoporous pores that made the Co-precursor easier to penetrate into the pores, increasing the opportunities for the reduced Co-nanoparticles to deposit not only on the outer surface but also the interior of the matrix, as illustrated in the inset of Fig. 2(a). The results indicate that there were smaller Co nanoparticles and better distribution in Co/SAG than in Co/MCM-41. Therefore, with the same weight of Co, Co/SAG was anticipated to provide more catalytic active-sites for the hydrolysis of ammonia borane than Co/MCM-41. The EDX spectra in Fig. S1† indicated the signals assigned to Co, Si and O elements in Co/SAG and Co/MCM-41, confirming that the reduced Co nanoparticles were successfully deposited to the SAG and MCM-41.

Fig. 3 shows the adsorption–desorption isotherms of the SAG, Co/SAG, MCM-41 and Co/MCM-41 powders. According to the IUPAC classification, all the samples exhibited type IV isotherms, indicating that they were all typical mesoporous materials.

The shapes of the hysteresis loops for SAG (Fig. 3(a)) and Co/SAG (Fig. 3(b)) as well as that for MCM-41 (Fig. 3(c)) and Co/MCM-41 (Fig. 3(d)) were similar and occurred at the same pressure, respectively, implying that the main structures of SAG and MCM-41 were remained before and after the Co deposition. However, the hysteresis loops of SAG and Co/SAG occurred at higher pressure than that of MCM-41 and Co/MCM-41, confirming that the mesopores were quite irregular and interconnected for SAG and Co/SAG, while that were regular mesopores as expected for MCM-41 and Co/MCM-41, in which the former is known to have hexagonal structure. The BET specific surface area, pore volume and average pore diameters of these powders were evaluated from the isotherms with the BET theory and Barrett–Joyner–Halenda (BJH) method. As listed in Table 1, the surface area, pore volume, and pore diameter of SAG obtained was 621 $m^2 g^{-1}$, 1.7 $cm^3 g^{-1}$, and 10.1 nm, respectively, and that of MCM-41 obtained was 798 $m^2 g^{-1}$, 0.7 $cm^3 g^{-1}$, and 2.9 nm, respectively. As expected for aerogels, the porosity and the pore diameter of SAG were much higher than that of MCM-41. This supports that the Co-precursor solution can penetrate into the mesopores of SAG more easily, providing more opportunity for the reduced Co particles to deposit not only the surface of SAG but also among the interior of the interconnected pores. On the contrary, due to the tiny pore size in MCM-41 the reduced Co nanoparticles were difficult to deposit into its mesopores. After the Co deposition, the value of surface area and pore volume, of Co/SAG was significantly changed to 449 $m^2 g^{-1}$, and 1.4 $cm^3 g^{-1}$, respectively, while that of Co/MCM-41 was only slightly changed to 741 $m^2 g^{-1}$ and 0.6 $cm^3 g^{-1}$, respectively. The changes of the surface area and pore volume for Co/SAG and Co/MCM-41 confirm that the Co nanoparticles were successfully deposited to SAG and MCM-41. The large decreases (27.7% decrease in the surface area and 17.6% in pore volume) for Co/SAG support that the deposition not only occurred on the surface but also among pores of the SAG matrix. However, the less changes (7.1% decrease in the surface area and 14.3% in pore volume) for Co/MCM-41 confirm that the Co deposition mainly occurred on the surface of MCM-41, forming larger particles but less affecting the morphology. On the other hand, because the pores in Co/SAG were much larger than that in Co/MCM-41, it was also anticipated that the NH_3BH_3 solution would be more easily diffuse in the pores of Co/SAG to react with the interior Co, leading to a more efficient hydrolysis to generate hydrogen.

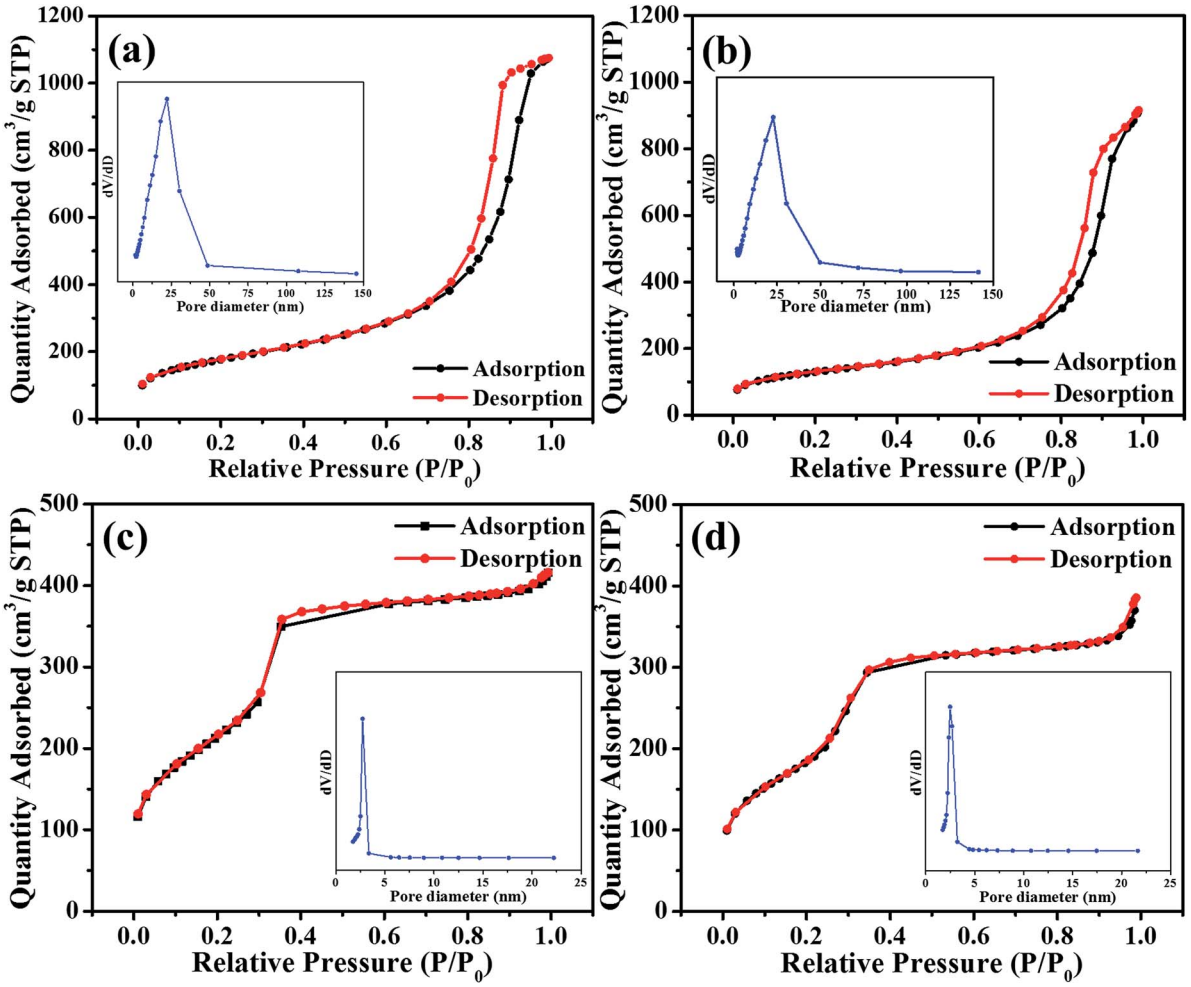

Fig. 3 Nitrogen adsorption–desorption isotherms of (a) SAG, (b) Co/SAG, (c) MCM-41 and (d) Co/MCM-41.

Table 1 BET Surface area, pore size and pore volume of the samples

Samples	Surface area ($m^2\ g^{-1}$)	Pore volume ($cm^3\ g^{-1}$)	Pore size (nm)
SAG	621	1.7	10.1
Co/SAG	449	1.4	12.3
MCM-41	798	0.7	2.9
Co/MCM-41	741	0.6	3.0

3.2 Hydrogen generation measurements

Fig. 4 shows the hydrogen generation profiles *vs.* time for the aqueous NH_3BH_3 (0.33 wt%) with various molar ratio of metal to NH_3BH_3 (M/AB) to evaluate the catalytic activities of the Co-based catalysts.

For comparison, the profiles for the AB solutions (0.33 wt%) containing the support but no Co showed no release of H_2 gas (Fig. 4) as the references. As can be seen, basically no hydrogen was released for the case without the metals, indicating that the SAG and MCM-41 were not catalysts for the hydrogen generation reaction. As listed in Table 2, the 0.33 wt% AB solution with M/AB = 0.05, the hydrogen generation was finished in 8 and 10 minutes in the presence of the Co/SAG and Co/MCM-41 catalysts, respectively. As the M/AB ratio was increased from 0.05 to 0.2, the hydrogen release rate with Co/MCM-41 catalyst changed from 3.9 to 11.1 ml min^{-1}, while that with Co/SAG catalyst increased from 4.9 to 15.6 ml min^{-1}. For M/AB = 0.2, the hydrogen generation rate obtained with the Co/SAG catalyst was about 41% higher than that with the Co/MCM-41 catalyst. The enhancement is ascribed to the smaller particle size and better distribution of the deposited Co nanoparticles in SAG than that in MCM-41, providing more catalytic sites for hydrolysis of the aqueous NH_3BH_3 as discussed above.

Fig. 5 illustrates the hydrogen generation under the catalysis of the Co-based catalysts at M/AB = 0.05 in the aqueous solution with various AB concentrations at 303 K. Fig. 5(a) indicates that the hydrogen release rates of the hydrolysis catalyzed by Co/SAG from the 0.33, 1.0 and 5.0 wt% AB solutions are 5.0, 4.98, and 5.0 (ml H_2 min^{-1}), respectively. This indicates that the hydrogen release rate is basically independent of the NH_3BH_3 concentration as shown in Fig. S2,† revealing a zero-order kinetic with respect to the substrate concentration for the hydrolysis catalyzed by Co/SAG as the study previously reported.[17]

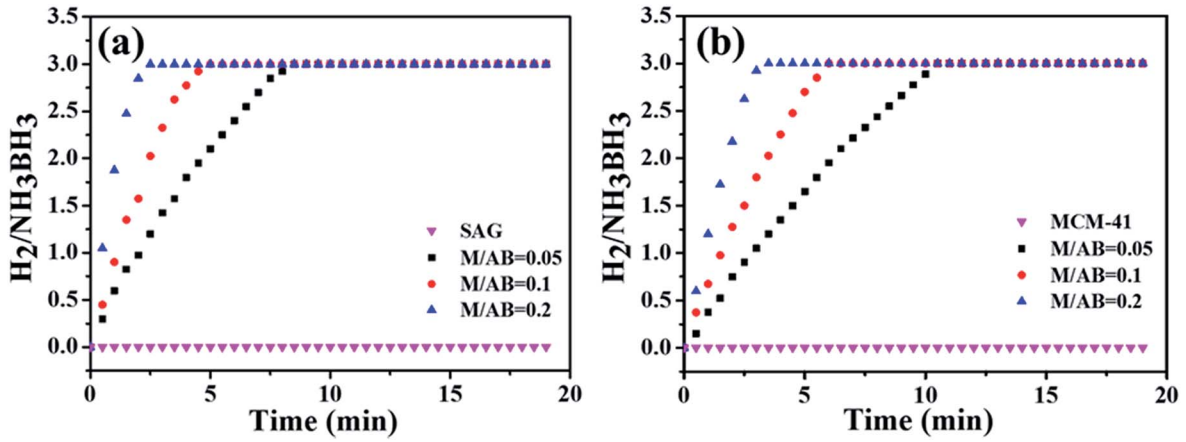

Fig. 4 Hydrogen generation from aqueous NH_3BH_3 (0.33 wt%) catalyzed by (a) Co/SAG and (b) Co/MCM-41 at 303 K under M/AB ratio from 0.05 to 0.2.

Table 2 Hydrogen generation (ml min^{-1}) from aqueous NH_3BH_3 (0.33 wt%) catalyzed by Co/SAG and Co/MCM-41 at 303 K under M/AB ratio from 0.05 to 0.2

	M/AB	
Catalyst	0.05	0.2
Co/MCM-41	3.9	11.1
Co/SAG	4.9	15.6

The hydrogen generation from the aqueous NH_3BH_3 (0.33 wt%) in the presence of Co/SAG under M/AB = 0.05 at different temperatures (303–323 K) is displayed in Fig. 6(a). As expected, the hydrolysis reaction was quickened with increasing temperature. To calculate its activation energy, the rate law and Arrhenius equation for the catalytic hydrolysis of aqueous NH_3BH_3 are given as the following equation.[18]

$$\frac{-1/3\mathrm{d}[NH_3BH_3]}{\mathrm{d}t} = \frac{\mathrm{d}[H_2]}{\mathrm{d}t} = k$$

Fig. 6(b) shows the Arrhenius plot, ln(k) *versus* the reciprocal absolute temperature.

The slope of the straight line gave the E_a value of 46.4 kJ mol^{-1} for Co/SAG. For comparison the turnover frequency (TOF) and activation energy (E_a) of different catalysts used for the hydrolytic dehydrogenation of ammonia borane,[18,31–41] are listed in Table 3. As can be seen, the E_a value of Co/SAG prepared in this study is lower than those of the most metal oxide-supported non-precious catalysts reported, such as Co/γ-Al_2O_3,[18] 1.2% Co@M41S[33] and Co–Ni–P/Pd–TiO_2,[40] implying that the hydrolytic dehydrogenation of ammonia borane can be easier taken place with Co/SAG as the catalyst. In addition, the TOF value of Co/SAG is also higher than most of the Co-based catalysts reported.[35–38] The results demonstrate that Co/SAG is able to function as an efficient non-precious catalyst towards hydrogen generation from aqueous ammonia borane.

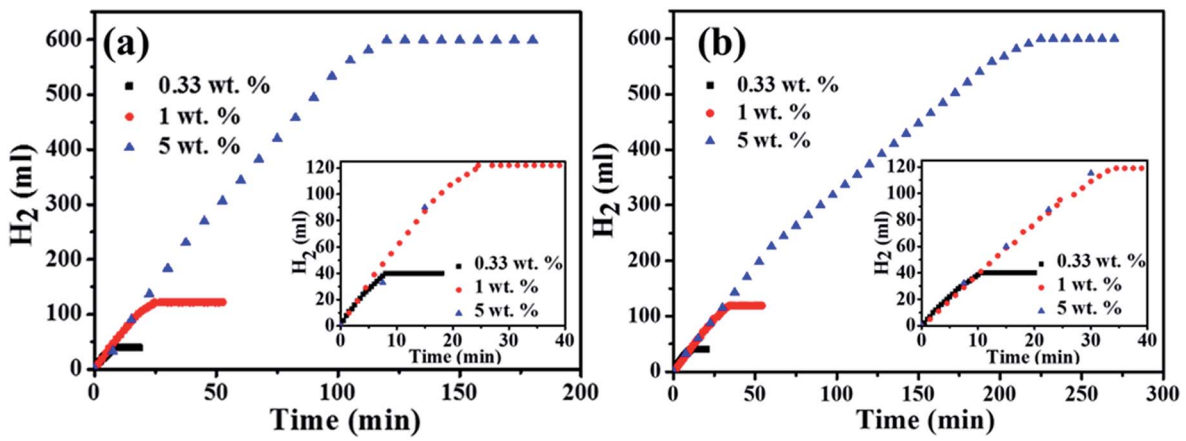

Fig. 5 Hydrolysis of various NH_3BH_3 concentration catalyzed by (a) Co/SAG and (b) Co/MCM-41 at 303 K with the catalyst amount kept unchanged.

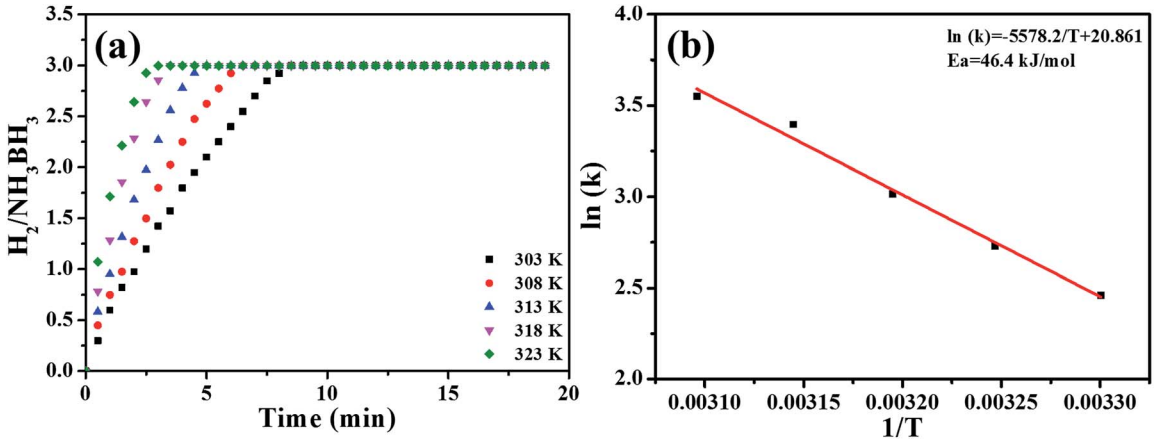

Fig. 6 (a) Time plots of catalytic dehydrogenation of aqueous NH_3BH_3 (0.33 wt%) over Co/SAG from 303 K to 323 K at M/AB = 0.05. (b) ln(k) *vs.* 1/*T* plot calculated from (a).

The favorable hydrogen generation from aqueous NH_3BH_3 by the catalysis with the Co supported interconnected porous SAG prepared in this study can be reasoned according to the mechanism reported by J. Chen *et al.*[32] The small Co nanoparticles deposited not only on the surface but among the interconnected mesopores in the SAG network structure, as shown in the TEM images above, provided more sites that could form the transient Co–H bonds, which were required for the hydrolysis of AB, consequently, increasing the opportunities for the H_2 generation.

3.3 Recyclability test

The recyclability of Co/SAG for hydrolysis of the aqueous NH_3BH_3 (0.33 wt%) was evaluated at 303 K and the corresponding plots are shown in Fig. 7. It is seen that the rates of hydrogen generation were not decayed from 1st to 3rd cycles. Even after five cycles, the H_2/NH_3BH_3 mole ratio of the dehydrogenation of NH_3BH_3 still retained to 3.0, indicating that the Co/SAG catalyst is an efficient catalyst for the hydrogen generation from aqueous NH_3BH_3. Similar cyclic phenomena have also been reported from the other non-precious catalysts.[23,42,43]

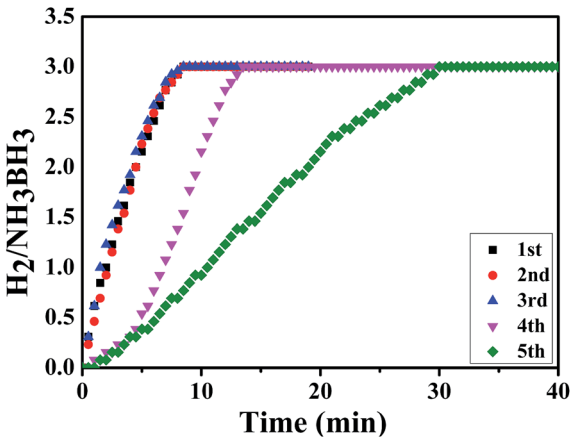

Fig. 7 Recyclability test of Co/SAG for hydrolysis of aqueous NH_3BH_3 (0.33 wt%) solution at 303 K where the M/AB value was 0.05.

Table 3 Values of turnover frequency (TOF) and activation energy (E_a) in different catalysts used for the hydrolytic dehydrogenation of ammonia borane

Catalysts	TOF (ml H_2 min^{-1} g^{-1} of metal)	E_a (kJ mol^{-1})	References
Co/γ-Al_2O_3	—	62.0	18
Ru@SiO_2	—	38.2	31
$Co_{0.32}$@$Pt_{0.68}$/C NPs	4874	41.5	32
1.2% Co@M41S	4378	54.6	33
Co–Cr–P–B	3325	44.0	34
Co–Mo–B	2460	43.0	35
Co–B/mesoporous silica	1150	—	36
$(Cu_{0.5}Co_{0.5})_2$Al-Cat	1000	—	37
Crystalline Co–B	394	46.2	38
Amorphous Co–B	376	47.5	38
Intrazeolite Co(0) nanoclusters	—	56.0	39
Co–Ni–P/Pd–TiO_2	—	54.9	40
NiCo–Pt	—	45.7	41
Co/SAG	3013	46.4	This study

4. Conclusion

In this study, the mesoporous silica aerogel-supported cobalt (Co/SAG) nanocomposite was successfully synthesized using a facile chemical reduction, employing sodium borohydride as the reducing agent at room temperature. The TEM micrograph revealed that Co nanoparticles with particle size less than 5 nm were homogenously deposited to Co/SAG. Co/SAG exhibited superior catalytic activity for hydrogen generation from the aqueous ammonia borane at ambient condition than Co/MCM-41 and exhibited a zero-order kinetics. The turnover frequency (TOF) and activation energy (E_a) were 3013 ml H_2 min^{-1} $g_{metal}{}^{-1}$ and 46.4 kJ mol^{-1}, respectively. The TOF value was higher and the E_a value was lower than the corresponding values of most of the Co-based catalysts reported for hydrolysis of the aqueous NH_3BH_3 solution. In addition, the Co/SAG catalyst was found recyclable for dehydrogenation of aqueous AB solution with retaining molar ratio of $H_2/NH_3BH_3 = 3.0$. These results indicate that the as-prepared silica aerogel-supported cobalt nanocomposite is an efficient catalyst for hydrogen generation from aqueous ammonia borane.

Acknowledgements

The authors would like to thank Chung Shan Institute of Science and Technology (CSIST-808-V314) and Chung Yuan Christian University of Taiwan (R.O.C.) for providing the financial support to this research work.

References

1 L. Schlapbach and A. Zuttel, *Nature*, 2001, **414**, 353.
2 D. Y. Xu, H. M. Zhang and W. Ye, *Catal. Commun.*, 2007, **8**, 1767.
3 L. Zhou, Y. Sun and Y. P. Zhou, *Chem. Eng. Commun.*, 2006, **193**, 564.
4 J. B. María, L. C. Dolores, S. G. Fabián, C. A. Diego and L. S. Ángel, *Microporous Mesoporous Mater.*, 2008, **112**, 235.
5 X. Ye, X. Gu, X. G. Gong, T. K. M. Shing and Z. F. Liu, *Carbon*, 2007, **45**, 315.
6 I. P. Jain, C. Lal and A. Jain, *Int. J. Hydrogen Energy*, 2010, **35**, 5133.
7 K. Doi, S. Hino, H. Miyaoka, T. Ichikawa and Y. Kojima, *J. Power Sources*, 2011, **196**, 504.
8 D. J. Collins and H. C. Zhou, *J. Mater. Chem.*, 2007, **17**, 3154.
9 Z. H. Lu and Q. Xu, *Funct. Mater. Lett.*, 2012, **5**, 1230001.
10 G. Xia, L. Li, Z. Guo, Q. Gu, Y. Guo, X. Yu, H. Liu and Z. Liu, *J. Mater. Chem. A*, 2013, **1**, 250.
11 W. R. H. Wright, E. R. Berkeley, L. R. Alden, R. T. Baker and L. G. Sneddon, *Chem. Commun.*, 2011, **47**, 3177.
12 H. Guo, X. Liu, Y. Hou, Q. Xie, L. Wang, H. Geng and D. L. Peng, *J. Power Sources*, 2014, **260**, 100.
13 Y. Tong, X. Lu, W. Sun, G. Nie, L. Yang and C. Wang, *J. Power Sources*, 2014, **261**, 221.
14 M. Chandra and Q. Xu, *J. Power Sources*, 2006, **156**, 190.
15 Ö. Metin, Ş. Şahin and S. Özkar, *Int. J. Hydrogen Energy*, 2009, **34**, 6304.
16 S. Basu, A. Brockman, P. Gagare, Y. Zheng, P. V. Ramachandran, W. N. Delgass and J. P. Gore, *J. Power Sources*, 2009, **188**, 238.
17 S. Çalışkan, M. Zahmakıran and S. Özkar, *Appl. Catal., B*, 2010, **93**, 387.
18 Q. Xu and M. Chandra, *J. Power Sources*, 2006, **163**, 364.
19 J. M. Yan, X. B. Zhang, S. Han, H. Shioyama and Q. Xu, *Angew. Chem., Int. Ed.*, 2008, **47**, 2287.
20 J. M. Yan, X. B. Zhang, H. Shioyama and Q. Xu, *J. Power Sources*, 2010, **195**, 1091.
21 J. Du, F. Cheng, M. Si, J. Liang, Z. Tao and J. Chen, *Int. J. Hydrogen Energy*, 2013, **38**, 5768.
22 Y. Yang, Z. H. Lu, Y. Hu, Z. Zhang, W. Shi, X. Chen and T. Wang, *RSC Adv.*, 2014, **4**, 13749.
23 X. Meng, S. Li, B. Xia, L. Yang, N. Cao, J. Su, M. He, W. Luo and G. Cheng, *RSC Adv.*, 2014, **4**, 32817.
24 Z. H. Lu, J. Li, G. Feng, Q. Yao, F. Zhang, R. Zhou, D. Tao, X. Chen and Z. Yu, *Int. J. Hydrogen Energy*, 2014, **39**, 13389.
25 S. B. Kalidindi, M. Indirani and B. R. Jagirdar, *Inorg. Chem.*, 2008, **47**, 7424.
26 A. C. Pierre and G. M. Pajonk, *Chem. Rev.*, 2002, **102**, 4243.
27 C. H. Tsai, F. L. Yang, C. H. Chang and Y. W. Chen-Yang, *Int. J. Hydrogen Energy*, 2012, **37**, 7669.
28 Y. W. Chen-Yang, C. W. Chen, Y. Z. Wu and Y. C. Chen, *Electrochem. Solid-State Lett.*, 2005, **8**, F1.
29 X. M. Liang and L. J. Zhao, *RSC Adv.*, 2012, **2**, 5485.
30 M. Chandra and Q. Xu, *J. Power Sources*, 2006, **159**, 855.
31 Q. Yao, W. Shi, G. Feng, Z. H. Lu, X. Zhang, D. Tao, D. Kong and X. Chen, *J. Power Sources*, 2014, **257**, 293.
32 X. Yang, F. Cheng, Z. Tao and J. Chen, *J. Power Sources*, 2011, **196**, 2785.
33 Y. C. Luo, Y. H. Liu, Y. Hung, X. Y. Liu and C. Y. Mou, *Int. J. Hydrogen Energy*, 2013, **38**, 7280.
34 R. Fernandes, N. Patel, A. Paris, L. Calliari and A. Miotello, *Int. J. Hydrogen Energy*, 2013, **38**, 3313.
35 R. Fernandes, N. Patel, A. Miotello, R. Jaiswal and D. C. Kothari, *Int. J. Hydrogen Energy*, 2012, **37**, 2397.
36 N. Patel, R. Fernandes, R. Edla, P. B. Lihitkar, D. C. Kothari and A. Miotello, *Catal. Commun.*, 2012, **23**, 39.
37 C. Li, J. Zhou, W. Gao, J. Zhao, J. Liu, Y. Zhao, M. Wei, D. G. Evans and X. Duan, *J. Mater. Chem. A*, 2013, **1**, 5730.
38 A. K. Figen and B. Coskuner, *Int. J. Hydrogen Energy*, 2013, **38**, 2824.
39 M. Rakap and S. Ozkar, *Int. J. Hydrogen Energy*, 2010, **35**, 3341.
40 M. Rakap, E. E. Kalu and S. Ozkar, *Int. J. Hydrogen Energy*, 2011, **36**, 254.
41 M. Wen, S. Zhou, Q. Wu, J. Zhang, Q. Wu, C. Wang and Y. Sun, *J. Power Sources*, 2013, **232**, 86.
42 Z. H. Lu, J. Li, A. Zhu, Q. Yao, W. Huang, R. Zhou, R. Zhou and X. Chen, *Int. J. Hydrogen Energy*, 2013, **38**, 5330.
43 X. Shan, J. Du, F. Cheng, J. Liang, Z. Tao and J. Chen, *Int. J. Hydrogen Energy*, 2014, **39**, 6987.

